Received: 20 January 2023 | Revised: 28 April 2023 | Accepted: 28 April 2023

DOI: 10.1111/jace.19245

Journal of the American Ceramic Society

RESEARCH ARTICLE

Viscous healing of Vickers indentation–induced cracks in glass

Carsten Blaeß | **Ralf Müller**

Department 5 Materials Engineering, Devision 5.6 Glasses, Bundesanstalt für Materialforschung und -prüfung (BAM), Berlin, Deutschland, Germany

Correspondence
Carsten Blaeß, Bundesanstalt für Materialforschung und -prüfung (BAM), Richard-Willstätter-Straße 11, 12489 Berlin, Germany.
Email: carsten.blaess@bam.de

Abstract

Viscous healing of cracks induced by the Vickers indentation in a soda lime magnesium silicate, a soda borosilicate, and a soda aluminosilicate glass (NAS) was studied by laser scanning microscopy. Plots of the crack length, width, and depth normalized to the initial crack length versus time over viscosity merge into single master curves of each of these quantities for each glass. Despite glass properties do not differ strikingly from each other, however, these master curves strongly differ among the glasses. This finding was attributed to a different interplay of various crack healing phenomena. Lateral cracks were found to be responsible for the bulging of the sample surface around the Vickers imprint, which in turn promotes radial crack widening as the main cause of healing delay. The most rapid healing of lateral cracks was observed in NAS in which bulging and crack widening were least pronounced.

KEYWORDS
crack healing, glass, Vickers indentation

1 | INTRODUCTION

Non-sufficient thermal cycling stability is a major obstacle to the large-scale application of solid oxide fuel cells (SOFC) with glass[1,2] or glass–ceramic sealants.[3–6] Their cycling stability is primarily threatened by stress-induced crack formation or delamination,[7–10] making them the most crucial failure component in SOFC stacks.[11,12] As such defects can partially close, refill, or completely disappear ("viscous healing") at the high operating temperature of SOFC stacks due to viscous flow,[8,13] studying such phenomena could help to improve stack lifetime.

Studies on crack healing are therefore of continuous interest.[13–15] Most studies have been based on the Vickers indentation technique, which allows radial cracks of limited size to be easily reproduced and readily described in terms of their length, L, width, W, and depth, D.[16–18] The viscous healing process of radial cracks was observed to include several stages: crack tip blunting,[19] rounding of the crack edges, widening[20] or grooving of radial cracks to form oval cavities or rounded open valleys, and their smoothing and filling.[21] Such phenomena have been reported for borosilicate,[22] magnesium–calcium silicate,[23] and soda lime silicate glasses.[24]

A kinetic description of viscous crack healing radial cracks induced by the Vickers indentation was given by Singh et al.[25,15] The authors based their concept on the analogy between crack healing and viscous sintering and found that the time required for complete healing of radial cracks scales with η/γ, where γ and η denote surface energy and glass viscosity, respectively.

Based on the same analogy, it was demonstrated in[26] for a soda lime magnesium silicate (NCMS) glass that crack healing progress scales with t/η, which is known for the initial[27] and final stage of viscous sintering.[28] Normalizing crack length $L(t)$ and width $W(t)$ with the initial radial crack length, L_0, allowed the plot of a master curve containing data across various Vickers indentations (different L_0) and isothermal healing temperatures (different η) on the same glass. This concept was later demonstrated in Ref. [29] by finite element simulation based on crack healing data reported in Ref. [26].

However, crack healing data for different glasses do not necessarily merge into the same master curve because γ and mechanical properties change with glass composition, and crack geometry varies greatly depending on the crack patterns induced by the Vickers indentation, for example, Palmqvist or Half-penny radial cracks and lateral cracks.[30–33] Therefore, in the present work, viscous radial crack healing in three different sodium silicate glasses is investigated. To prevent surface crystallization during viscous crack healing, only glasses for which low crystallization tendency could be deducted from literature[26,34,35] were selected.

2 | EXPERIMENTAL PROCEDURES

2.1 | Glasses

The first glass, NCMS, is a commercial NCMS microscopic slide glass (VEB Technisches Glas Ilmenau, Germany). Its suitability for crack healing experiments has been demonstrated in.[26] The other two, a sodium borosilicate glass (NBS) and a sodium aluminosilicate glass (NAS), were melted from reagent grade SiO_2 (Elkem, Oslo, Norway), H_3BO_3 (Carl Roth, Karlsruhe, Germany), Na_2CO_3, γ-Al_2O_3, $BaCO_3$ (Merck, Darmstadt, Germany), and ZrO_2 (3-YTZ-E, Tosoh, Tokyo, Japan) raw materials. Both glass compositions, NBS and NAS, were chosen because of their low crystallization tendency and glass transition temperature of around 550°C reported in Refs. [34] and [35]. NBS was melted as a 4-kg batch in a 2-L Pt crucible at 900°C (pre-melt) and then at 1500°C for 1.5 h in an inductive middle-frequency furnace (V 2001 0959, EMA-TEC, Sondershausen, Germany). Hereby, glass homogeneity was improved by 30 min stirring. NAS was melted as a 450 g batch at 1450°C (pre-melt) and finally at 1600°C for 2.5 h in a 200 mL Pt crucible in a conventional electric furnace.

Glass plates of both glasses were prepared by casting the melt onto steel plates and slowly cooling from 600°C to room temperature in a muffle furnace (MLW, VEB Elektro, Bad Frankenhausen, Germany). The glass NCMS was used as received.

2.2 | Methods

Glass composition was measured on three bulk glass samples each using XRF (Zetium Ultimate, Malvern Panalytical, Almelo, the Netherlands) with a 4 kW Rh radiation source. The relative error depending on the measured element/calculated oxide was smaller than 3%. Glass density, ρ, was measured on glass pieces of different dimensions using the Archimedes method in deionized water at 23°C using the balance Kern 770 (Kern & Sohn, Germany).

The calorimetric glass transition temperature, $T_{g\text{-}DTA}$, was characterized by differential thermal analysis (TAG24, Setaram, Caluire, France). Measurements were conducted at 10 K/min in synthetic air (45 mL/min) on bulk samples (≈33 mg) in uncovered Pt crucibles. The coefficient of thermal expansion, $\alpha_{20\text{–}300°C}$, the dilatometric glass transition temperature, $T_{g\text{-}Dil}$, and dilatometric softening temperature, $T_{S\text{-}Dil}$, were determined with a horizontal dilatometer (DIL 402c, Netzsch, Germany) using cylindrical samples 25 mm in length and 4–6 mm in diameter and heated at 5 K/min from 20 to 800°C.

Glass viscosity was measured by means of rotational concentric cylinder viscometry (VT550, Haake, Vreden, Germany) for $\eta < 10^5$ Pa s, beam bending viscometry on bars of $14 \times 0.8 \times 12$ mm^3 for $\eta = 10^{12}$–10^9 Pa s, and cylinder compression tests by parallel plate viscometry on drilled cores with dimensions of ≈5.5 mm in height and diameter for the range $\eta = 10^9$–10^7 Pa s. The latter two methods were performed by means of a high-temperature vertical dilatometer TMA 801 (TA instruments, Hüllhorst, Germany). Samples of NCMS for parallel plate viscometry and beam bending were drilled and cut out of five plates after sintering together for 30 min at 750°C (10 K/min).

The specific glass melt surface energy at 900°C, γ, was roughly estimated in a first approximation from the following equation according to Ref. [36] and as demonstrated in Ref. [37] where γ_i is the surface energy contribution, and wt_i is the weight fraction of glass components:

$$\gamma = \sum \gamma_i wt_i \quad (1)$$

The possible maximum error of γ was estimated by comparing with the data of Lyon[38] to be less than 10%. Crack healing in NCMS was studied on glass plates of $11 \times 11 \times 1$ mm^3, which were prepared from the as-received microscopic slide glass plates of $76 \times 26 \times 1$ mm^3 by diamond scratching and manual fracture. NBS and NAS glass plates of the same size were achieved by cutting with a diamond saw, grinding (SiC-grinding disks), and polishing (3 and 1 μm diamond suspension).

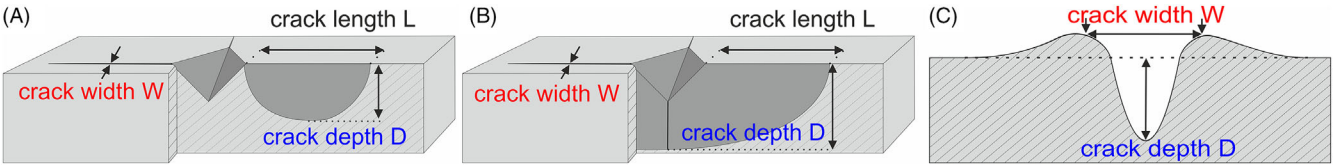

FIGURE 1 Schematic representation of measured crack size data length, L, width, W, and depth, D for (A) Palmqvist cracks, (B) half-penny cracks, and (C) cross section of a widened radial crack at the half of its length.

Cracks were generated by the Vickers indentation using an INNOVATEST micro Vickers (Innovent, Maastricht, the Netherlands) loaded with 19.62 N for a dwell time of 10 s. Indentations were 1 mm apart. For healing studies, however, only indentations with three or four radial cracks, one per imprint corner, were chosen. This way, around 100 suitable radial cracks per sample are included in every data point.

Crack healing progress was monitored by means of stepwise isothermal heat treatments in an electrical tube furnace in air at 20%–35% RH. As moisture can influence both the crack healing rate in soda lime glass[39,24] as well as the sintering,[40] the moisture was kept constant within reasonable fluctuation. For each sample, a fluctuation of ≤5% RH was realized. For crack healing experiments, a temperature range of 580–682°C was chosen. This range corresponds to a viscosity of $10^{6.8}$–$10^{10.1}$ Pa s, which is typical of the range of early sintering[41] and which also makes sure that residual stresses are fully relaxed. The used in-house built tube furnace provides a homogeneous temperature field (±1 K at 660°C across the sample) and permits short sample insertion times. Samples reach the furnace temperature within 70–103 s depending on their size. After each heat treatments (varied between 30 and 120 min for different viscosity), the sample was freely cooled to room temperature, and the healing progress of the Vickers indentations and radial cracks was monitored by confocal laser scanning microscopy (LSM) using a LEXT OLS4100 (Olympus, Tokyo, Japan). Crack length (L), width (W), and depth (D) were measured using the software ImageJ[42] according to Figure 1. Statistical outliers were identified and excluded by the boxplot method. It was assumed that residual stresses during cooling did not have significant effects on L, W, and D due to the crack tip blunting expected already during the first annealing step.

3 | RESULTS

3.1 | Glass properties

Glass composition and property data are listed in Tables 1 and 2. Although the silicate glass NCMS, the borosilicate glass NBS, and the aluminosilicate glass NAS essentially

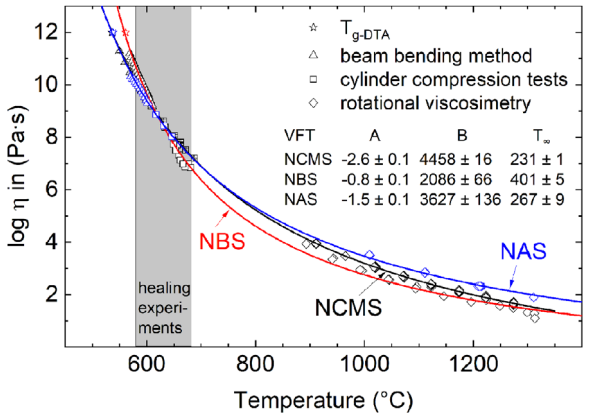

FIGURE 2 Glass viscosity measured by beam bending method (△), cylinder compression tests (□), rotational viscometry (◇), and DTA (☆, T_g at $\eta = 10^{12}$ Pa s). Curves are Vogel–Fulcher–Tammann (VFT) fits using parameter mentioned in Equation (2) in Pa s and °C.

differ in their glass-forming constituents, their glass transition and softening temperatures do not differ more than 30 K. On the other hand, NBS sticks out in all properties, most particularly with its low density, estimated surface energy, and thermal expansion coefficient.

Viscosity data are visualized in Figure 2 from beam bending (△), cylinder compression (□), rotational viscometry (◇), and DTA (☆), where $T_{g\text{-}DTA}$ is attributed to $\eta = 10^{12}$ Pa s.[43,44] Curves are best fits with the empirical Vogel–Fulcher–Tammann (VFT) equation[37]:

$$\log \eta = A + B(T - T_\infty)^{-1} \quad (2)$$

A more thorough glass physical interpretation of Equation (2) is given in Ref. [45]. Although the temperature dependence of viscosity slightly differs for the glasses under study, these differences are marginal in the viscosity–temperature range of crack healing experiments.

3.2 | Crack patterns

Consistent with Table 2, broadly similar crack patterns were caused by the Vickers indentation. The top row in Figure 3 shows LSM images of typical examples. For all

TABLE 1 Glass composition measured by XRF with a relative error <3%.

Glass	Composition (mol%)											
	SiO_2	B_2O_3	Al_2O_3	Na_2O	K_2O	MgO	CaO	Y_2O_3	BaO	HfO_2	ZrO_2	Others
NCMS	67.50	–	0.50	14.97	0.26	10.11	6.66	–	–	–	–	–
NBS	62.46	17.50	0.04	14.74	0.01	–	0.01	0.15	–	0.06	4.92	0.11
NAS	65.55	–	10.30	23.30	–	–	–	–	0.86	–	–	–

Abbreviations: NAS, sodium aluminosilicate; NBS, sodium borosilicate; NCMS, soda lime magnesium silicate.

TABLE 2 Glass properties: calorimetric glass transition temperature, $T_{g\text{-}DTA}$, dilatometric glass transition temperature, $T_{g\text{-}Dil}$, dilatometric softening temperature, $T_{S\text{-}Dil}$, coefficient of thermal expansion, $\alpha_{20\text{–}300°C}$, density, ρ, surface energy, γ.

Glass	$T_{g\text{-}DTA}$ (°C)	$T_{g\text{-}Dil}$ (°C)	$T_{S\text{-}Dil}$ (°C)	$\alpha_{20\text{–}300°C}$ (10^{-6} K^{-1})	ρ (g/cm^3)	γ (m N/m)
NCMS	538 ± 3	536 ± 2	607 ± 2	9.18 ± 0.09	2.47 ± 0.02	336
NBS	561 ± 2	559 ± 2	615 ± 2	7.47 ± 0.09	2.30 ± 0.10	270
NAS	538 ± 2	536 ± 1	606 ± 1	10.70 ± 0.22	2.50 ± 0.01	335

Abbreviations: NAS, sodium aluminosilicate; NBS, sodium borosilicate; NCMS, soda lime magnesium silicate.

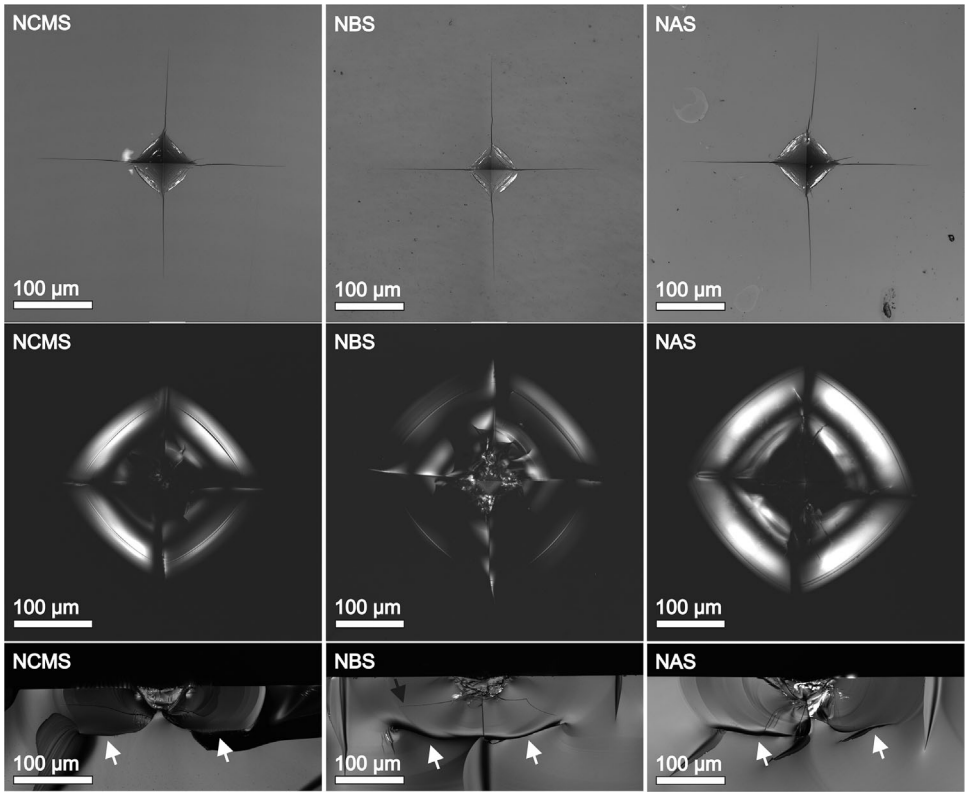

FIGURE 3 Laser scanning microscopy (LSM) images of typical Vickers indentation–induced cracking patterns for the glasses under study. The top row shows LSM images focused on the glass surface, the middle line shows LSM images focused on lateral cracks beneath the surface, and the bottom row shows samples manually fractured along radial cracks after the Vickers indentation.

glasses, the initial radial crack length, L_0, is nearly equal (127 ± 6, 131 ± 4, and 129 ± 9 μm for NCMS, NBS, and NAS, respectively). For NBS, however, the pyramidal imprint is smaller. The middle row, for which the LSM has been focused beneath the surface, shows the similar occurrence of lateral cracks. These cracks are also seen (white arrows) in the bottom row, which shows samples manually fractured along the radial cracks after the Vickers indentation. As known from the literature,[32] lateral cracks (white arrows) occurred beneath the Vickers imprint after the radial cracks had formed. This row also reveals that for NCMS and NAS, radial cracks are formed on either side of the indentation as "Palmqvist cracks,"[31] whereas for NBS, the radial cracks are merged into each

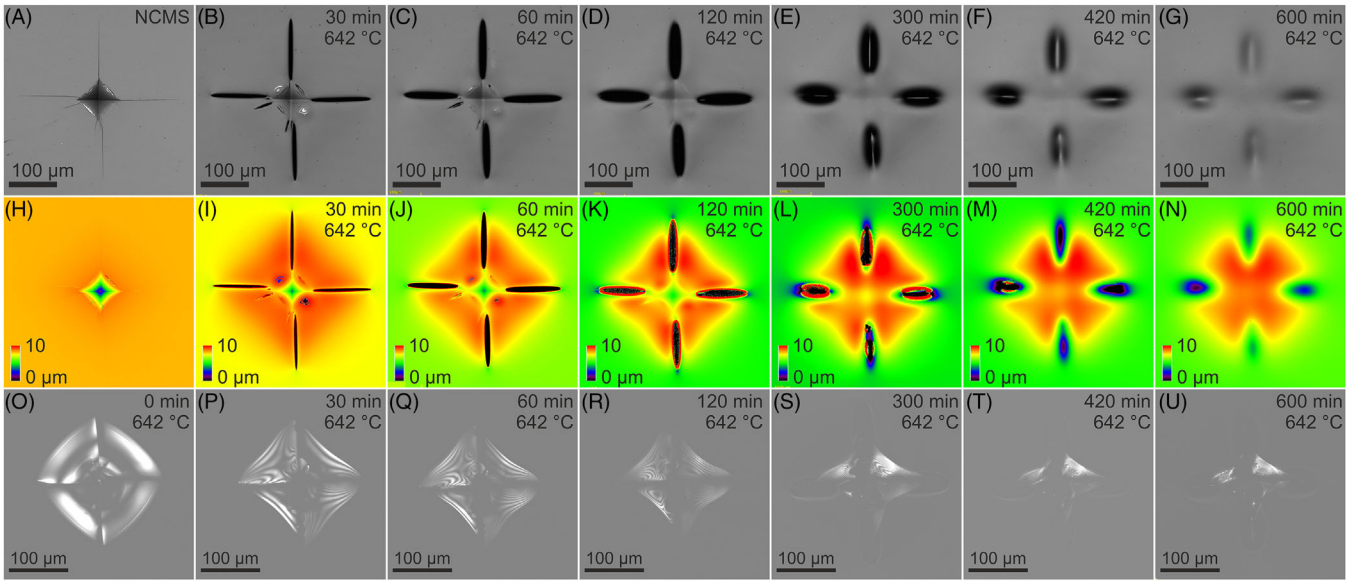

FIGURE 4 Laser scanning microscopy (LSM) images from different crack healing stages in NCMS at 642°C ($\eta = 10^{8.2}$ Pa s). Top row (A–G): LSM focused on the glass surface. Middle row (H–N): Height profiles. Bottom row (O–U): LSM focused on lateral cracks beneath the surface.

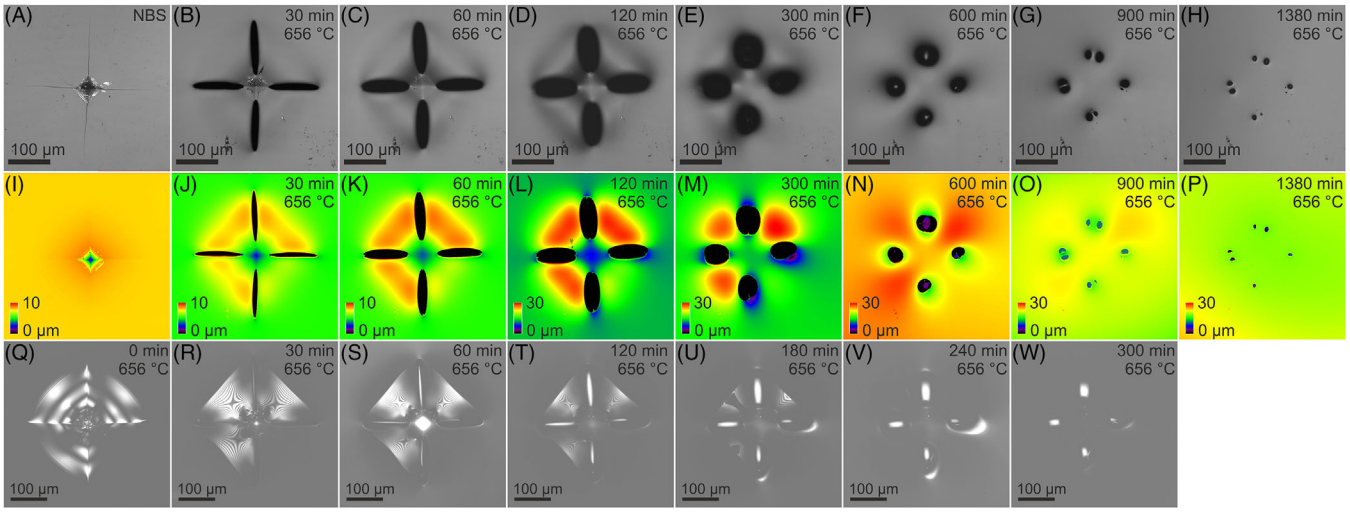

FIGURE 5 Laser scanning microscopy (LSM) images from different stages of crack healing in sodium borosilicate glass (NBS) at 656°C ($\eta = 10^{7.5}$ Pa s). Top row (A–H): LSM focused on the glass surface. Middle row (I–P): Height profiles. Bottom row (Q–W): LSM focused on lateral cracks beneath the surface.

other below the indentation to a "Halfpenny" crack.[31] As a third particularity of NBS, secondary lateral cracks are evident (black arrow).

3.3 | Crack healing phenomena

Figures 4–6 depict LSM micrographs from different stages of isothermal healing of representative Vickers indentations for each studied glass. As a common trend, it is shown that radial cracks undergo some widening while decreasing their length and the Vickers imprint is filled (top rows, Figures 4A–G, 5A–H, 6A–H). The bottom rows (Figures 4O–U, 5Q–W, 6Q–W) show that the lateral cracks simultaneously disappear as well. The colored height profiles (middle row, Figures 4H–N, 5I–P, 6I–P) reveal substantial bulging of the four glass segments located between the radial cracks in almost any case.

Despite these common trends, crack healing progress differs across the different glasses. In NCMS, radial cracks

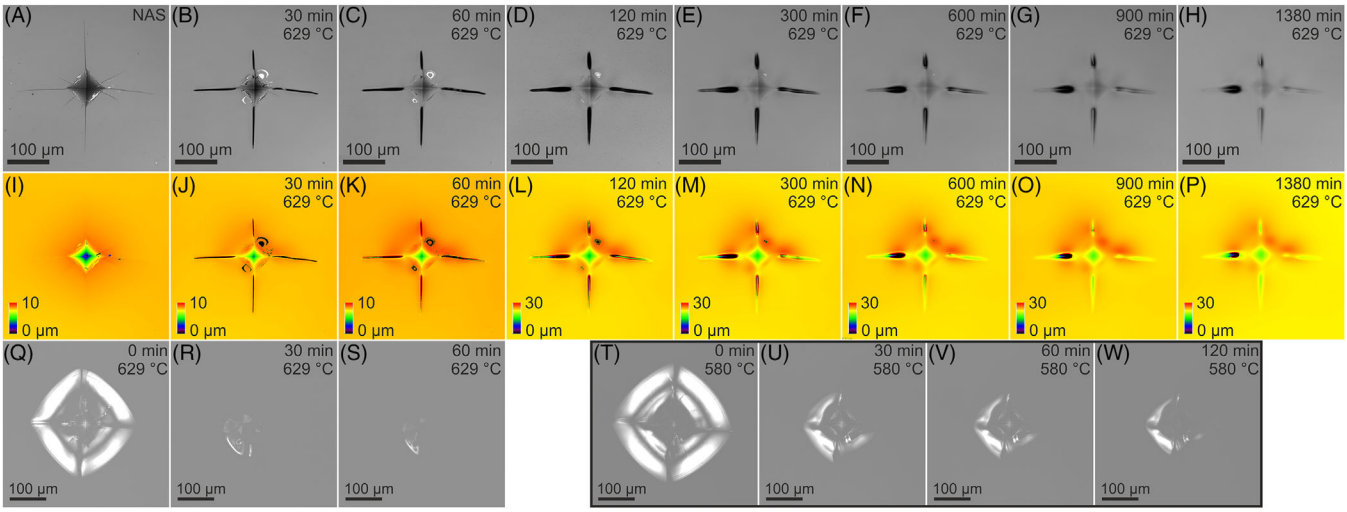

FIGURE 6 Laser scanning microscopy (LSM) images from different stages of crack healing in sodium aluminosilicate (NAS) at 629°C ($\eta = 10^{8.5}$ Pa s). Top row (A–H): LSM focused on the glass surface. Middle row (I–P): Height profiles. Bottom row (Q–W): LSM focused on lateral cracks beneath the surface. The lateral crack healing at 629°C (Q–S) was already complete at 60 min. Lateral crack healing was therefore also observed at 580°C ($\eta = 10^{10.1}$ Pa s) (T–W) for another Vickers indentation.

widen moderately to oval cavities (Figure 4B–F) and later smooth to plane oval valleys (Figure 4G). Initially, bulging is most pronounced along the radial crack edges stretching from their inner tip (at the Vickers imprint corner) to their center (e.g., Figure 4K). Later, these bulging maxima tend to merge into each other (e.g., Figure 4M, upper segments). Possibly affected by bulging phenomena, the filled Vickers imprint rises above glass surface level in late stages of healing (Figure 4LM).

In contrast, NBS shows more pronounced crack widening (Figure 5). Rounded radial cracks form broad and almost circular cavities (Figure 5M–P). The Vickers imprint raises only slightly above surface level after being filled. Similar to NCMS, bulging within the segments is most pronounced near the radial crack edges, whereas the bulging maxima later merge into each other in the center of the different segments. However, in contrast to NCMS, the position of the bulging maximum is located further away from the imprint at the center of the radial crack cavity (Figure 5M). Interestingly, the upper and left cavities split into two separated pores during progressive healing (Figure 5O,P), whereas the lower and right cavities do not.

In NAS, the effect of segment bulging and crack widening is least pronounced, and the surface cavities remain small, narrow, and elongated (Figure 6A–H,I–P). Most of them disappear completely before any significant filling of the Vickers imprint is evident. This peculiarity is accompanied by the strongest pronounced and earliest decrease in the length of radial cracks. Both phenomena also correlate with the most rapid disappearance of lateral cracks beneath the Vickers imprint, which were therefore studied at lower temperatures (42 K instead of 91 K above T_g, Figure 6M–R).

3.4 | Radial crack healing kinetics

Figure 7 illustrates the healing progress in terms of the radial crack length, L, width, W, and depth, D, normalized to the initial radial crack length L_0. In this way, crack size data from different Vickers imprints and different annealing temperatures can be presented within a single master plot,[26] and more reliable conclusions can be drawn about similarities and differences in crack healing among the glasses studied. Although radial crack depth information is not shown in Figures 4–6, D was measured with LSM beyond a certain degree of crack widening.

As a common trend, Figure 7 shows that the steady decrease in relative radial crack length L/L_0 and crack depth D/L_0 are initially accompanied by crack opening and widening, that is, an increase in W/L_0. For NCMS and NBS, L/L_0 and W/L_0 reach similar values close to about 0.4 during the maximal crack opening, at which time the crack cavities reach a spherical shape in the glass surface and thus have minimized their surface area within this dimension. For NAS (Figure 7C), this time point is not reached. Although L/L_0 and W/L_0 also aspire to similar values, L/L_0 decreases to ≈0.3, whereas W/L_0 does not surpass 0.15. As observed for NCMS (Figure 7A), healing is completed when D/L_0 approaches zero, whereas L/L_0 and W/L_0 do not. This situation indicates shallow cavities or valleys during the late healing stages for NCMS

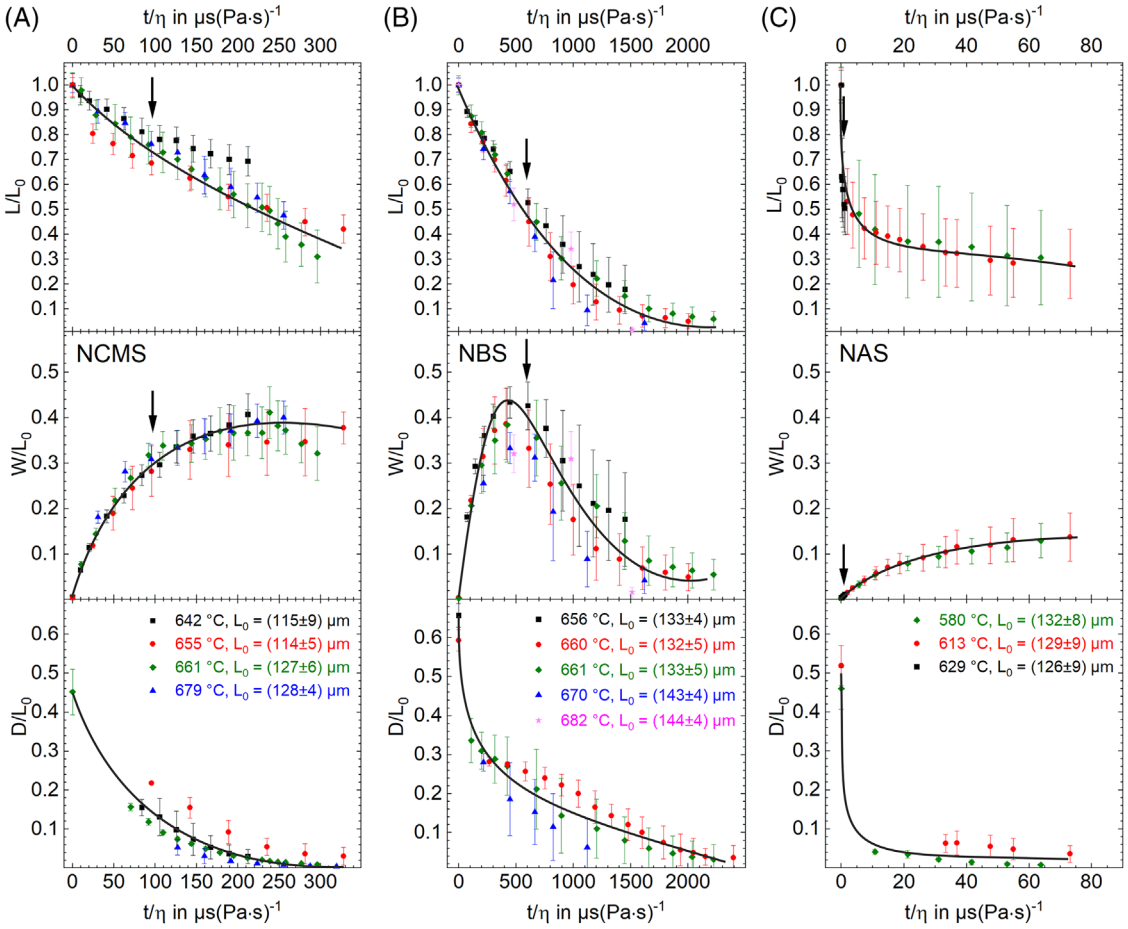

FIGURE 7 Isothermal healing progress in terms of the relative radial crack length L/L_0, width W/L_0, and depth D/L_0 at different temperatures versus t/η for NCSM (A), NBS (B), and NAS (C). Black arrows mark the disappearance of lateral cracks. Curves are guides for the eye.

and NAS (compare Figures 4G and 6F). In contrast, L/L_0, W/L_0, and D/L_0 disappear almost simultaneously for NBS in Figure 7B indicating almost spherical cavities.

Another significant difference in crack healing is the disappearance of lateral cracks. These cracks are indicated by downward-pointing black arrows in Figure 7. The disappearance of lateral cracks occurs exceptionally fast for NAS. Another striking feature of NAS is that both L/L_0 and D/L_0 decrease rapidly during the initial thermal treatment. Thus, the initial crack depth decreases by almost 90% by the first measurable data point.

4 | DISCUSSION

4.1 | Crack healing phenomena

Figures 4–6 illustrate the complexity of simultaneous phenomena in the healing of Vickers indentations and induced radial and lateral cracks. The Vickers imprint is steadily filled by viscous flow, while radial cracks widen before being filled starting from their former outer crack tip. The lateral cracks, located beneath the Vickers indentation, were also closed. At the same time, the volume segments separated from each other by the radial cracks and separated from the interior of the glass by lateral cracks beneath them bulge and rise to different degrees, whereas radial crack edges are getting progressively rounded.

The crack widening and rounding hinder the healing of radial crack length in two ways. On the one hand, crack tip blunting slows healing, similar to the way the sintering of glass powders slows with increasing neck radius. On the other hand, in wide-opened cracks, more space is available during healing, which must be filled by viscous flow. In contrast, the healing of narrow cracks requires much less viscous transport.

Figure 7 already indicated that the healing of radial cracks strongly depends on the presence of lateral cracks. This effect is easy to understand, because radial and lateral cracks divide the glass around the Vickers imprint into different segments. These segments are separated from each other by radial cracks and cut off from the glass inte-

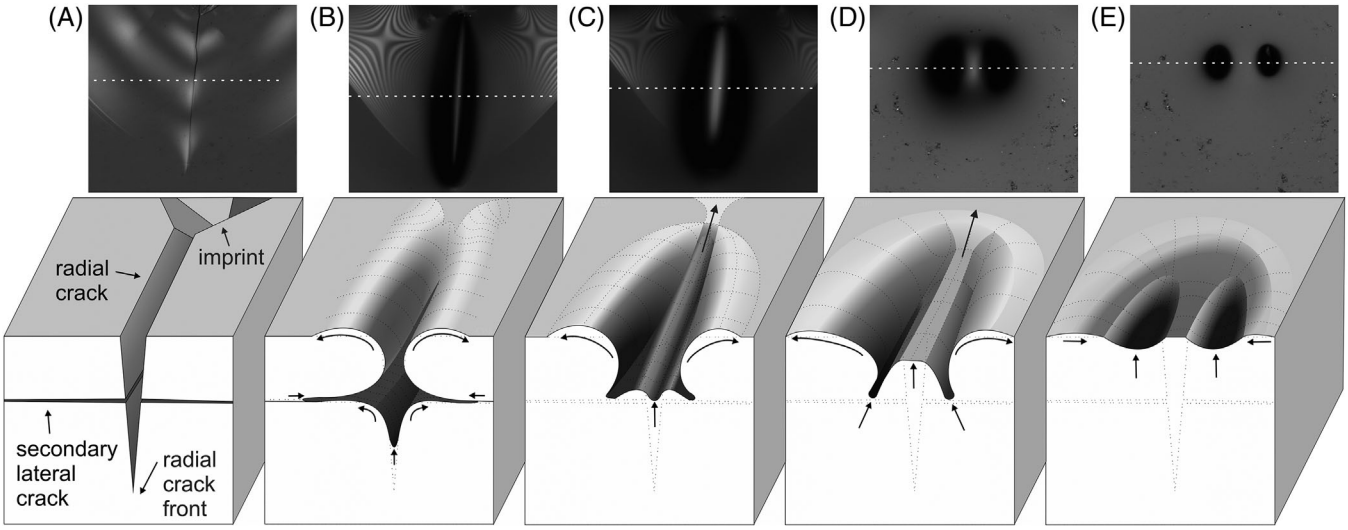

FIGURE 8 Hypothetical explanation of the evolution of double cavities during radial crack healing. Micrographs in the upper row illustrate the relevant healing stage for the left radial crack shown in Figure 5 (combined and rotated micrographs). Primary lateral cracks, marked with white arrows in Figure 3, are not drawn here. Arrows indicate expected viscous flow patterns. (A) Radial and lateral crack as recieved after Vickers indentation, (B) initial widening of radial crack and healing of lateral crack, rounding of crack edges, (C) further widening and rounding, (D) rising of fomer radial crack tip, (E) formation of separated cavities.

rior by lateral cracks underneath. This partial isolation may explain the pronounced bulging of these segments, as less viscous flow is required to minimize their surface-to-volume ratio. This correlation is supported in Figures 4–6 by the coincidence between the presence of lateral cracks and the degree of bulging. Figure 5 (NBS) even shows the absence of any bulging in the lower right segment, where no lateral crack is evident.

The bulging could be additionally supported by the presence of secondary lateral cracks as indicated for NBS in Figure 3. These cracks are located between the glass surface and other lateral cracks (white arrows). In this way, upper volume segments are cut off from the lower one, which leads to a decrease in their surface-to-volume ratio. As this upper segment is smaller, less viscous material transport or a shorter time is required to approach a rounded shape. Although Figure 3 shows only one example Vickers indentations, secondary lateral cracks have been observed in other samples and may be responsible for the fact that rapid bulging and pronounced crack widening is a general trend for NBS, as seen in Figure 7B.

Although no strict reason can be given on the present data basis, Figure 8 offers a hypothetical explanation for the curious appearance of two cavities instead of one at the final stage of radial crack healing in NBS (Figure 5). This effect is counterintuitive as two cavities would result in a larger surface-to-volume ratio than one. As the core idea, Figure 8A assumes the presence of secondary lateral cracks, as shown in Figure 3. These cracks subdivide the radial crack and its neighboring glass segments into a top and bottom layer. This effect additionally should promote the bulging and crack widening of the top segments as discussed above. The resulting enhanced viscous flow perpendicular to the radial crack may explain the observed pronounced crack widening, and the shallow residual secondary lateral crack can explain the cavity profile deviation across the radial crack from a simple minimum shape in this dimension. However, along the radial crack extension, this effect does not matter. Along this dimension, the former radial crack tip rises, as shown in Figure 8D, driven by the decreasing surface area (upper arrows) and as would occur for a single cavity. These differences in surface curvature perpendicular and parallel to the former radial crack could explain the observed symmetry breaking during crack healing and the formation of double cavities in the final healing stage. Of course, without further investigation, this hypothetical explanation cannot be proven based solely on the observations presented. However, it may be useful as an impetus for further research and as a stimulus for future discussion.

4.2 | Crack healing kinetics

Figure 7 confirms previous observations on NCMS[26] and first shows that crack healing data measured for the same glass for different Vickers indentations and healing temperatures converge to single master curves of L/L_0, W/L_0, and D/L_0 versus t/η.

However, for different glasses, strong differences in healing kinetics can be seen in Figure 9, which shows representative crack healing data of Figure 7 to scale. In

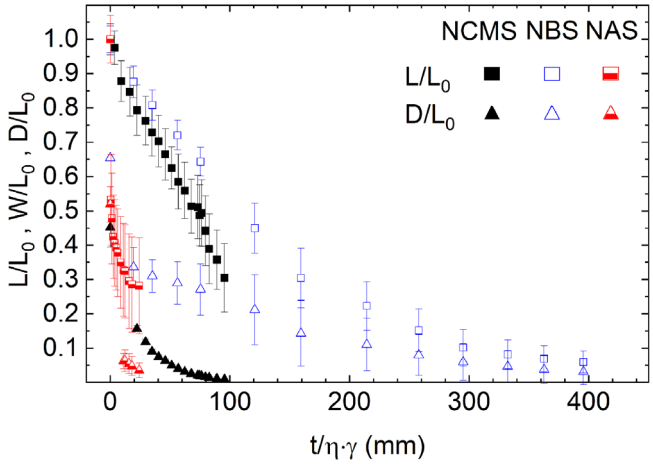

FIGURE 9 Representative L/L_0, W/L_0, and D/L_0 data taken from Figure 7 versus $t/\eta{\cdot}\gamma$ shown to scale.

comparison, complete crack healing in Figure 7 occurs 4 and 29 times faster in NAS than that in NCMS and NBS, respectively ($t/\eta \approx 75$, 300, and 2200 μs/(Pa s) for NAS, NCMS, and NBS, respectively). Even an extended master curve concept in Figure 9, including γ, would fail because of the outstanding healing capability of NAS, as can be seen in Figure 9. Thus, γ deviates by only ≈20% (Table 2), whereas t/η differs by a factor of 8 ($t/\eta{\cdot}\gamma \approx 25$ and 400 for NAS and NBS, respectively) for complete healing. The similar γ reflects the rather similar glass properties of NCMS and NCS shown in Table 2. This similarity in glass properties and the observed distinct differences in crack healing capability indicate that crack healing is not entirely dominated by η and γ.

On the other hand, there is also no obvious consistent correlation with the observed initial crack patterns. However, secondary lateral cracks can explain the lower crack healing capability of NBS, and although similar early crack length healing of NBS and NCMS occurs, the factor of 4 faster complete crack healing in NAS than in NCMS (Figure 9) cannot be explained in this way, as Figure 2 and Table 2 show quite similar crack geometry, η and γ for these two glasses.

This difficulty might be related to the fact that the bulk properties were considered, and γ was estimated from glass composition data. However, the surface properties may differ greatly. For example, it is known that sodium ions can be enriched on the fracture surface[46,47] and on the surface of glass melts.[37] In addition, water adsorbs rapidly on the freshly fractured surface and can fill narrow cavities, possibly creating a specific microclimate inside the crack[48,49] or even closing it.[50] Water may even diffuse into the glass interior and accumulate just below the fractured surface.[51–54] In all cases, a near-surface decrease in viscosity is to be expected, as is known, for example, from sintering in humid atmosphere.[40] For the highly shielded inner regions of radial and lateral cracks, this increased near-surface mobility due to diffusion may not fully relax during heating and may affect at least the early stage of crack healing. Furthermore, healing of radial cracks from the crack front can be supported by capillary-driven viscous flow.[21]

As NAS has the highest sodium content, it may be most susceptible to surface sodium accumulation and corrosion phenomena due to water entrapment. Therefore, locally reduced viscosity at the fractured surface could explain the rapid healing of the lateral cracks even after the first heat treatment (first data points in Figure 7C), which later minimizes crack widening ($W(t)/L_0 < 0.2$) and thus a rapid healing of radial cracks.

Another effect is related to the fact that the observed crack patterns do not fully reveal the crack geometry or shape. Thus, half-penny cracks were found in NBS, whereas two semicircular Palmqvist cracks were found for NCMS and NAS. Although all crack dimension data were always normalized by L_0, different D_0/L_0 ratios, that is, the crack geometry, can affect the crack healing kinetics. Thus, the finite element simulation in Ref. [31] showed that the time to reach a certain value of L/L_0 is $\sim D_0{\cdot}\eta/\gamma$. Nevertheless, the similar initial decrease of L/L_0 for NBS and NCMS could be explained by the fact that the shape of the half-penny cracks in NBS is essentially different from a semicircular shape.

5 | SUMMARY

The viscous healing of radial and lateral cracks induced by the Vickers indentation was investigated on an NCMS, an NBS, and an NAS glass. As earlier demonstrated for NCMS,[26] normalized crack healing data for different Vickers indentations and healing temperatures (L/L_0, W/L_0, and D/L_0) plotted versus t/η also resulted in single master curves for NAS and NBS as well. However, all three master curves strongly differ from each other, although glass properties do not differ strikingly. Thus, crack healing was 4 and 29 times faster in NAS than that in NCMS and NBS, respectively.

It was shown that this effect reflects a different interplay between various crack healing phenomena. Thus, the shortening of radial crack length is temporarily inhibited by its widening, as the associated increase in crack tip curvature and crack volume slows crack healing. This widening was additionally promoted by the bulging of the four glass segments separated by radial cracks and cut off from below by lateral cracks. In this situation, less viscous transport is required to minimize the local surface-to-volume ratio. Widening of radial cracks and bulging

was almost completely suppressed for NAS, for which an exceptionally rapid healing of lateral cracks. Conversely, the intensity of widening and bulging was most pronounced for NBS, where shallow secondary lateral cracks were observed between the surface and underlying lateral cracks. In this case, widening and bulging of the top segmental layer is additionally promoted.

ACKNOWLEDGMENTS

We gratefully acknowledge experimental support by our colleague from BAM, C. Meyer, for viscosity determination assistance and dilatometric measurements.

Open access funding enabled and organized by Projekt DEAL.

CONFLICT OF INTEREST STATEMENT

The authors identify no conflict of interest.

ORCID

Carsten Blaeß https://orcid.org/0000-0001-5620-2005

REFERENCES

1. Fergus JW. Sealants for solid oxide fuel cells. J Power Sources. 2005;147(1–2):46–57.
2. Mahapatra MK, Lu K. Seal glass for solid oxide fuel cells. J Power Sources. 2010;195(21):7129–39.
3. Schwickert T, Sievering R, Geasee P, Conradt R. Glass-ceramic materials as sealants for SOFC applications. Materialwiss Werkstofftech. 2002;33(6):363–6.
4. Reis ST, Brow RK. Designing sealing glasses for solid oxide fuel cells. J Mater Eng Perform. 2006;15(4):410–3.
5. Pascual MJ, Guillet A, Durán A. Optimization of glass–ceramic sealant compositions in the system MgO–BaO–SiO_2 for solid oxide fuel cells (SOFC). J Power Sources. 2007;169(1):40–6.
6. Gross SM, Federmann D, Remmel J, Pap M. Reinforced composite sealants for solid oxide fuel cell applications. J Power Sources. 2011;196(17):7338–42.
7. Selçuk A, Merere G, Atkinson A. The influence of electrodes on the strength of planar zirconia solid oxide fuel cells. J Mater Sci. 2001;36(5):1173–82.
8. Singh RN. Sealing technology for solid oxide fuel cells (SOFC). Int J Appl Ceram Technol. 2007;4(2):134–44.
9. Atkinson A, Sun B. Residual stress and thermal cycling of planar solid oxide fuel cells. Mater Sci Technol. 2007;23(10):1135–43.
10. Kuhn B, Wessel E, Malzbender J, Steinbrech RW, Singheiser L. Effect of isothermal aging on the mechanical performance of brazed ceramic/metal joints for planar SOFC-stacks. Int J Hydrogen Energy. 2010;35(17):9158–65.
11. Batfalsky P, Malzbender J, Menzler NH. Post-operational characterization of solid oxide fuel cell stacks. Int J Hydrogen Energy. 2016;41(26):11399–411.
12. Zhang YC, Lu MJ, Jiang WC, Tu ST, Zhang XC. Effect of the geometrical size on time dependent failure probability of the solid oxide fuel cell. Int J Hydrogen Energy. 2019;44(21):11033–46.
13. Doquet V, Ben Ali N, Chabert E, Bouyer F. Experimental and numerical study of crack healing in a nuclear glass. Mech Mater. 2015;80:145–62.
14. Cheeseman GL, Lawn BR. Artificial healing of cone cracks in glass. Phys Status Solidi A. 1970;3(4):951–8.
15. Rao P, Singh RN. Kinetics of crack healing and self-repair behaviors in a sealant glass for SOFC applications. Int J Appl Ceram Technol. 2022;19(6):3149–57.
16. Haranoh T, Ishikawa H, Shinkai N, Mizuhashi M. Crack evolution in Vickers indentation for soda-lime silica glass. J Mater Sci. 1982;17(5):1493–500.
17. Sglavo VM, Bertoldi M. Vickers indentation: a powerful tool for the analysis of fatigue behavior on glass. Ceram Trans. 2004;156:13–22.
18. Kiefer P, Deubener J, Muller R, Behrens H. Statistical analysis of propagation rates of indentation-induced radial cracks in soda-lime-silica glass. J Non-Cryst Solids. 2020;527:119739.
19. Hirao K, Tomozawa M. Kinetics of crack tip blunting of glasses. J Am Ceram Soc. 1987;70(1):43–8.
20. Kese KO, Li ZC, Bergman B. Contact residual stress relaxation in soda-lime glass Part II. Aspects relating to strength recovery. J Eur Ceram Soc. 2006;26(6):1013–22.
21. Hrma P, Han WT, Cooper AR. Thermal healing of cracks in glass. J Non-Cryst Solids. 1988;102(1–3):88–94.
22. Wilson BA, Case ED. In situ microscopy of crack healing in borosilicate glass. J Mater Sci. 1997;32(12):3163–75.
23. Chladek J, Muller R, Weh L, Reinsch S. Viscous flow and surface crystallization caused by Vickers indentation. Glass Sci Technol. 2004;77(1):1–6.
24. Girard R, Faivre A, Despetisz F. Influence of water on crack self-healing in soda-lime silicate glass. J Am Ceram Soc. 2011;94(8):2402–7.
25. Singh RN. Kinetics of self-repair in inorganic glasses: modeling and experimental verification. J Mater Sci. 2014;49(14):4869–79.
26. Blaeß C, Müller R. Master curve for viscous crack healing. Mater Lett. 2018;216:110–2.
27. Frenkel J. Viscous flow of crystalline bodies under the action of surface tension. J Phys (Moscow). 1945;9:385–91.
28. Mackenzie JK, Shuttleworth R. A phenomenological theory of sintering. Proc Phys Soc, Sect B. 1949;62:833–52.
29. Kanchika S, Wakai F. A model of crack healing of glass by viscous flow at elevated temperatures. J Am Ceram Soc. 2019;102(3):1373–8.
30. Whittle BR, Hand RJ. Morphology of Vickers indent flaws in soda-lime-silica glass. J Am Ceram Soc. 2001;84(10):2361–5.
31. Cook RF, Pharr GM. Direct observation and analysis of indentation cracking in glasses and ceramics. J Am Ceram Soc. 1990;73(4):787–817.
32. Cook RF, Liniger EG. Kinetics of indentation cracking in glass. J Am Ceram Soc. 1993;76(5):1096–105.
33. Duval A, Houizot P, Rouxel T. Review: elaboration, structure, and mechanical properties of oxynitride glasses. J Am Ceram Soc. 2022;106(3):1611–37
34. Pascual MJ, Pascual L, Duran A, Wange P, Russel C. Alumina and zirconia as inhibitors of crystallization during sintering of borosilicate glasses. Glass Sci Technol. 2002;75(2):69–74.
35. Muramoto T, Araya S, inventors; Central Glass Co Ltd, assignee. Glass for press forming and substrate glass for information recording medium. Japan patent JP2000319036A. 2000.
36. Dietzel A. Praktische Bedeutung und Berechnung der Oberflächenspannung von Gläsern, Glasuren und Emails. Sprechsaal. 1942;75:82–5.

37. Scholze H. Glas: Natur, Struktur und Eigenschaften. Berlin, Heidelberg, New York: Springer; 1988. p. 410.
38. Lyon KC. Calculation of surface tensions of glasses. J Am Ceram Soc. 1944;27(6):186–9.
39. Wilson BA, Case ED. Effect of humidity on crack healing in glass from in-situ investigations using an ESEM. J Mater Sci. 1999;34(2):247–50.
40. Cutler IB. Effect of water vapor on sintering of glass powder compacts. J Am Ceram Soc. 1969;52(1):11–3.
41. Müller R, Reinsch S. Viscous-phase silicate processing. In: Bansal NP, Boccaccini AR, editors. Ceramics and composites processing methods. Hoboken: John Wiley & Sons; 2012. p. 75–144.
42. Schneider CA, Rasband WS, Eliceiri KW. NIH image to ImageJ: 25 years of image analysis. Nat Methods. 2012;9(7):671–5.
43. Mazurin OV. Problems of compatibility of the values of glass transition temperatures published in the world literature. Glass Phys Chem. 2007;33(1):22–36.
44. Mazurin OV, Gankin YV. Glass transition temperature: problems of measurement procedures. Glass Technol: Eur J Glass Sci Technol, A. 2008;49(5):229–33.
45. Gutzow I. The thermodynamic function of supercooled glass forming liquids and the temperature dependence of their viscosity. In: Douglas RW, Ellis B, editors. Amorphous Materials: Papers Presented to the Third International Conference on the Physics of Non–Crystalline Solids Held at Sheffield University. London: Wiley–Interscience; 1972. p. 159–170.
46. Langford SC, Jensen LC, Dickinson JT, Pederson LR. Alkali emission accompanying fracture of sodium-silicate glasses. J Mater Res. 1991;6(6):1358–68.
47. Célarié F, Ciccotti M, Marliere C. Stress-enhanced ion diffusion at the vicinity of a crack tip as evidenced by atomic force microscopy in silicate glasses. J Non-Cryst Solids. 2007;353(1):51–68.
48. Weissmann R. Oberflächencharakterisierung, thermisches und chemisches Vorspannen und physikalische Beschichtungsverfahren von Glas. In: Peters A, Schaeffer HA, Weissmann R, Beier W, editors. Veränderung und Veredelung von Glasoberflächen – HVG-Fortbildungskurs 1989. Frankfurt/Main: Verlag der Deutschen Glastechnischen Gesellschaft; 1989. Chap. III, p. 1–40.
49. Baptist R, Levy F. Carbon-dioxide adsorption on glass. Vacuum. 1992;43(3):213–4.
50. Michalske TA, Fuller ER. Closure and repropagation of healed cracks in silicate glass. J Am Ceram Soc. 1985;68(11):586–90.
51. Nogami M, Tomozawa M. Diffusion of water in high silica glasses at low-temperature. Phys Chem Glasses. 1984;25(3):82–5.
52. Tomozawa H, Tomozawa M. Diffusion of water into a borosilicate glass. J Non-Cryst Solids. 1989;109(2–3):311–7.
53. Wakabayashi H, Tomozawa M. Diffusion of water into silica glass at low-temperature. J Am Ceram Soc. 1989;72(10):1850–5.
54. Tomozawa M, Kim DL, Agarwal A, Davis KM. Water diffusion and surface structural relaxation of silica glasses. J Non-Cryst Solids. 2001;288(1–3):73–80.

How to cite this article: Blaeß C, Müller R. Viscous healing of Vickers indentation–induced cracks in glass. J Am Ceram Soc. 2023;106:5795–5805. https://doi.org/10.1111/jace.19245